arXiv:1610.06039v1 [nucl-th] 17 Oct 2016

Production of φ-mesons on nuclear targets in the Quark-Gluon String model

G.H. Arakelyan[1], C. Merino[2], Yu.M. Shabelski[3]

[1]A.Alikhanyan National Scientific Laboratory
(Yerevan Physics Institute)
Yerevan, 0036, Armenia
e-mail: argev@mail.yerphi.am

[2]Departamento de Física de Partículas, Facultade de Física
and Instituto Galego de Física de Altas Enerxías (IGFAE)
Universidade de Santiago de Compostela
15782 Santiago de Compostela
Galiza-Spain
e-mail: merino@fpaxp1.usc.es

[3]Petersburg Nuclear Physics Institute
NCR Kurchatov Institute
Gatchina, St.Petersburg 188350, Russia
e-mail: shabelsk@thd.pnpi.spb.ru

Abstract

We consider the experimental data on φ-meson production on nuclear targets, and we find that they present unusually small shadow corrections for the inclusive density in the midrapidity region. We also give a quantitatively consistent description of both the initial energy dependence and the A-dependence of the produced φ-mesons, obtained in the frame of the Quark-Gluon String Model.

PACS. 25.75.Dw Particle and resonance production

1 Introduction

The experimental data on the production of φ-mesons, a rarely produced system formed of $s\overline{s}$ quarks, in proton-nucleus and nucleus-nucleus collisions show at very high energies unusually small shadow correction effects in the midrapididty region.

In this paper we discuss a possible reason for this effect that takes into account the fact that though s and $\overline{s}$ quarks have non-zero masses, at the same time their masses are not large enough to make standard perturbative Quantum Chromodynamics applicable, what could allow the treatment of the φ-meson as an intermediate case between soft and hard physics. We present the corresponding theoretical results, obtained by using the formalism of the Quark-Gluon String Model (QGSM) [1, 2].

This model has been successfully used for the description of multiparticle production processes in hadron-nucleon [1, 2], hadron-nucleus [3, 4] and nucleus-nucleus [5, 6] collisions. The QGSM description of the production of secondary pseudoscalar mesons π and K, and of baryons p, $\overline{p}$, Λ, and $\overline{\Lambda}$, was obtained many years ago in [7, 8, 9, 10]. Vector meson production was considered in [11, 12, 13, 14]. The yields of hyperons, including the multistrange ones, has been described in [15, 16].

In the case of collisions with a nuclear target, the saturation of the inclusive density of secondaries [15] found at very high energies was also successfully described by QGSM [15, 17, 18, 19].

Already in the paper [14] we had for the first time applied the QGSM formalism to the description of the spectra of vector φ-mesons production in πp and pp collisions, and of the ratios of yields φ/π^- and φ/K^- in pp collisions for a large scope of the initial energy, going up to the RHIC and LHC ranges.

In this paper we extend our analysis to the production of φ-mesons in high-energy collisions on a nuclear target, and we provide a consistent description of the small shadow correction effects measured for this case in the midrapididty region.

2 Meson inclusive spectra in the QGSM

In order to produce quantitative results for the integrated over p_T inclusive spectra of secondary hadrons, a model for multiparticle production is needed. It is for that purpose that we have used the QGSM [1, 2] in the numerical calculations presented below.

The QGSM [1, 2], based on the Dual Topological Unitarization, Regge phenomenology, and nonperturbative notions of QCD, has been used for already more than thirty years to succesfully predict and describe many features of the hadronic processes in a wide energy range. In particular, the QGSM allows one to make quantitative predictions on the inclusive densities of different secondaries produced at high energy collisions both in the central and beam fragmentation regions.

In the QGSM, the high energy hadron-nucleon, hadron-nucleus, and nucleus-nucleus

interactions are treated as proceeding via the exchange of one or several Pomerons, and all elastic and inelastic processes result from cutting through or between Pomerons [20]. Each Pomeron corresponds to a cylinder diagram (see Fig. 1a), in which the cylinder boundaries are drawn by the dash-dotted vertical lines. The surface of the cylinder is schematically depicted by dashed lines, while the solid lines at the top and bottom of the cylinder represent, respectively, the beam and the target quarks, which interaction is mediated by the Pomeron exchange.

The cut through the cylinder produces two showers of secondaries, i.e. quark-antiquark pairs shown in Fig 1b by solid lines. The inclusive spectrum of secondaries is then determined by the convolution of diquark, valence quark, and sea quark distributions in the incident particles, $u(x,n)$, with the fragmentation functions of quarks and diquarks into the secondary hadrons, $G(z)$. Both functions $u(x,n)$ and $G(z)$ are determined by the appropriate Reggeon diagrams [21]. Note that the quark-antiquark distributions $u(x,n)$ differ from the standard PDF's extracted from fits to experimental data because the $u(x,n)$'s are theoretically taken to be valid at the rather low Q^2 which are relevant for soft processes, while the PDF distributions are obtained by fixing the behavior at large Q^2. The diquark and quark distribution functions depend on the number n of cut Pomerons in the considered diagram. For the following calculations we have used the prescription given in reference [3].

For a nucleon target, the inclusive rapidity, y, or Feynman-x, x_F, spectrum of a secondary hadron h has the form [1]:

$$\frac{dn}{dy} \;=\; \frac{x_E}{\sigma_{inel}} \cdot \frac{d\sigma}{dx_F} \;= \sum_{n=1}^{\infty} w_n \cdot \phi_n^h(x) \;, \tag{1}$$

where the functions $\phi_n^h(x)$ determine the contribution of diagrams with n cut Pomerons and w_n is the relative weight of this diagram. Here, for the φ-meson production in the midrapidity region, we neglect the contribution of diffraction and dissociation processes.

In the case of pp collisions:

$$\begin{aligned} \phi_n^h(x) &= f_{qq}^h(x_+,n)\cdot f_q^h(x_-,n) + f_q^h(x_+,n)\cdot f_{qq}^h(x_-,n) \\ &+ 2(n-1)\cdot f_s^h(x_+,n)\cdot f_s^h(x_-,n) \;\;, \qquad (2) \\ x_\pm &= \frac{1}{2}[\sqrt{4m_T^2/s + x^2} \pm x] \;\;, \qquad (3) \end{aligned}$$

where f_{qq}, f_q, and f_s correspond to the contributions of diquarks, valence quarks, and sea quarks, respectively.

These contributions are determined by the convolution of the diquark and quark distributions with the fragmentation functions, e.g.,

$$f_q^h(x_+,n) = \int_{x_+}^1 u_q(x_1,n) G_q^h(x_+/x_1) dx_1 \;\;. \tag{4}$$

In the calculation of the inclusive spectra of secondaries produced in pA collisions we should consider the possibility of one or several Pomeron cuts in each of the ν blobs of

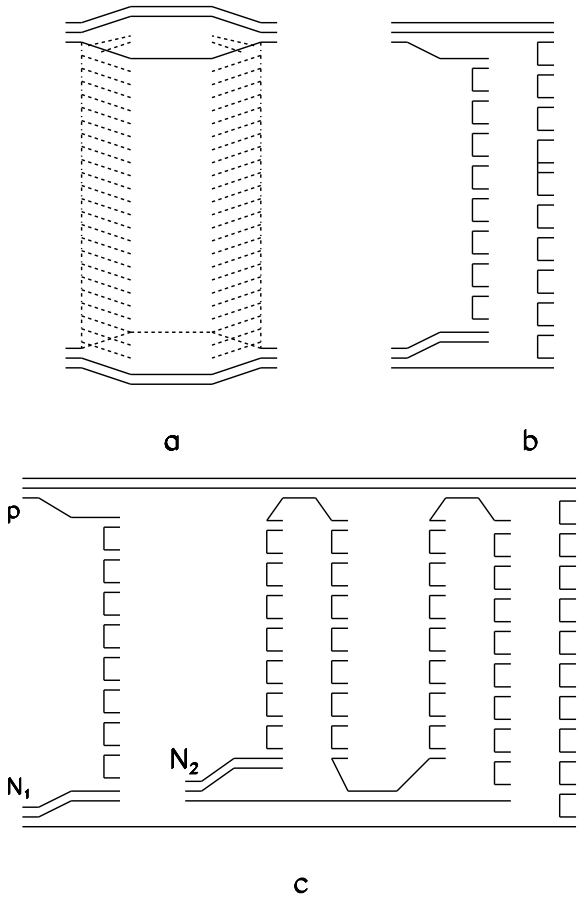

Figure 1: (a) Cylindrical diagram representing the Pomeron exchange within the Dual Topological Unitarization (DTU) classification (quarks are shown by solid lines); (b) Cut of the cylindrical diagram corresponding to the single-Pomeron exchange contribution in inelastic pp scattering; (c) Diagram corresponding to the inelastic interaction of an incident proton with two target nucleons N_1 and N_2 in a pA collision.

the proton-nucleon inelastic interactions. For example, in Fig. 1c it is shown one of the diagrams contributing to the inelastic interaction of a beam proton with two nucleons from the target. In the blob of the proton-nucleon$_1$ interaction one Pomeron is cut, and in the blob of the proton-nucleon$_2$ interaction two Pomerons are cut. It is essential to take into account all the diagrams with every possible Pomeron configuration and its permutations. The diquark and quark distributions and the fragmentation functions here are the same as in the case of the interaction with one nucleon.

The process shown in Fig. 1c satisfies [22, 23, 24, 25] the condition that the absorptive parts of the hadron-nucleus amplitude are determined by the combination of the absorptive parts of the hadron-nucleon amplitudes.

In the case of a nucleus-nucleus collision, in the fragmentation region of the projectile we use the approach [5, 26, 27], where the beam of independent nucleons of the projectile interacts with the target nucleus, what corresponds to the rigid target approximation [28] of Glauber Theory. In the target fragmentation region, on the contrary, the beam of independent target nucleons interacts with the projectile nucleus,

these two contributions coinciding in the central region. The corrections for energy conservation play here a very important role if the initial energy is not very high. This approach was used in [27] for the successful description of $\pi^{\pm}$, $K^{\pm}$, p, and $\overline{p}$ produced in PbPb collisions at 158 GeV/c per nucleon.

We use in this paper the values of the Pomeron parameters in ref. [8], and the fragmentation functions of quarks and diquarks into φ-meson are presented in ref. [14].

3 The φ-meson production in pA collisions

We will start from the case of φ-meson production in pA collisions. The experimental data obtained by the HERAb Collaboration at $\sqrt{s} = 41.6$ GeV [29] are presented in Table 1 and Fig. 2.

Reactions	Experimental data $d\sigma_{pA}/dy$, $\|y\| \leq 0.5$	QGSM
p + C	1.74 ± 0.15	1.5
p + Ti	6.85 ± 0.7	7.1
p + W	23.5 ± 2.1	19.1

Table 1: The experimental data for φ-mesons production in pA collisions at $\sqrt{s} = 41.6$ GeV by the HERAb Collaboration [29], together with the corresponding QGSM results.

Due to the AGK cancel rules [20], the inclusive cross section $d\sigma/dy$ in midrapidity region should present a linear A-dependence:

$$d\sigma_{pA}/dy(y \simeq 0) = A \cdot d\sigma_{pp}/dy(y \simeq 0) \ . \tag{5}$$

Some numerically small corrections to this linear behaviour are connected to the energy conservation rule when the initial energy is not high enough [22]. One can see in Fig. 2 that these corrections are really small at the energy $\sqrt{s} = 41.6$ GeV (the difference between the solid and the dashed curves is small for a very large range of A).

Also in ref. [29], the rapidity distribution of inclusive cross section for φ-mesons production in pA collisions are presented for rather small rapidity ranges. The existing experimental points, together with the results of the QGSM calculations, are shown in Fig. 3. The comparison between theory and experiment seems to be good.

4 The φ-meson production in heavy ion collisions up to RHIC energies

In the case of production of such a particles as pions and kaons, which give the main contribution to the mean multiplicity at energies starting from $\sqrt{s} = 40{-}60$ Gev,

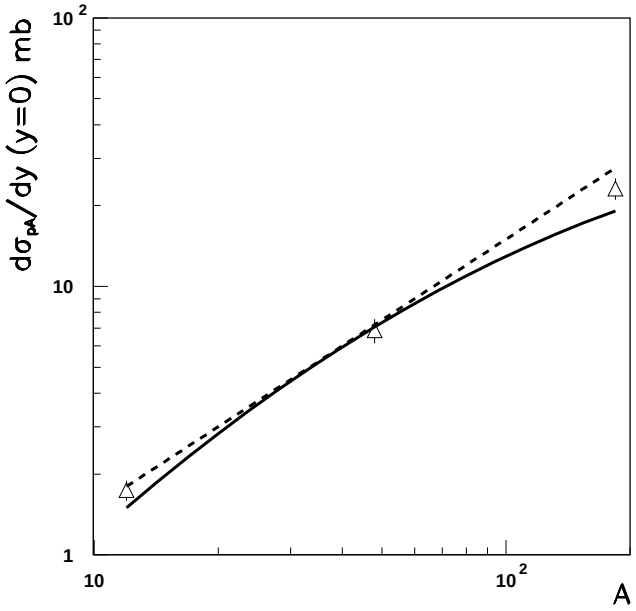

Figure 2: The experimental data on the A-dependence of $d\sigma_{pA}/dy(y \simeq 0)$ of produced φ-mesons in pA collisions at $\sqrt{s} = 41.6$ Gev [29], together with the corresponding QGSM results (solid curve), and with the linear dependence $d\sigma/dy \propto A^1$ (dashed straight line).

new shadowing effects appear [30] (see next section). On the contrary, in the case of φ-mesons production these shadowing effects are absent, even for the whole RHIC energy range, only appearing at LHC energies, as it will be discussed in detail in the next section.

Now, we will consider the φ-mesons production in heavy ion collisions at energies from $\sqrt{s}$=17 GeV to $\sqrt{s}$=200 GeV.

The existing experimental data on midrapidity inclusive densities for produced φ-mesons by the NA49 Collaboration ($\sqrt{s}$=17.3 Gev [31]) and those obtained at RHIC (STAR and PHENIX collaborations, $\sqrt{s}$=62.4 Gev [32], $\sqrt{s}$=130 Gev [33, 34], and $\sqrt{s}$=200 Gev [32, 35]) are presented in Table 2.

Reactions	Centrality	Energy $\sqrt{s}$ GeV	Experimental data dn/dy, $\|y\| \leq 0.5$	QGSM
Pb + Pb	0−5%	17.3	2.35 ± 0.15, [31]	2.764
Au + Au	0−20%	62.4	3.52 ± 0.08 ± 0.45, [32]	3.36
Au + Au	0−11%	130.	5.73 ± 0.37, ± 0.57, [33, 34]	6.15
Au + Au	0−5%	200.	7.95 ± 0.11 ± 0.73, [32]	7.57
Au + Au	0−5%	200.	7.70 ± 0.30, [35]	7.57

Table 2: The experimental data on dn/dy, $|y| \leq 0.5$, of φ-mesons production in different central nucleus-nucleus collisions at different energies, together with the corresponding QGSM results.

The experimental energy dependence of dn/dy (y=0) is presented in Fig. 4, together with the result of the QGSM calculation. The rather strong energy dependence of this

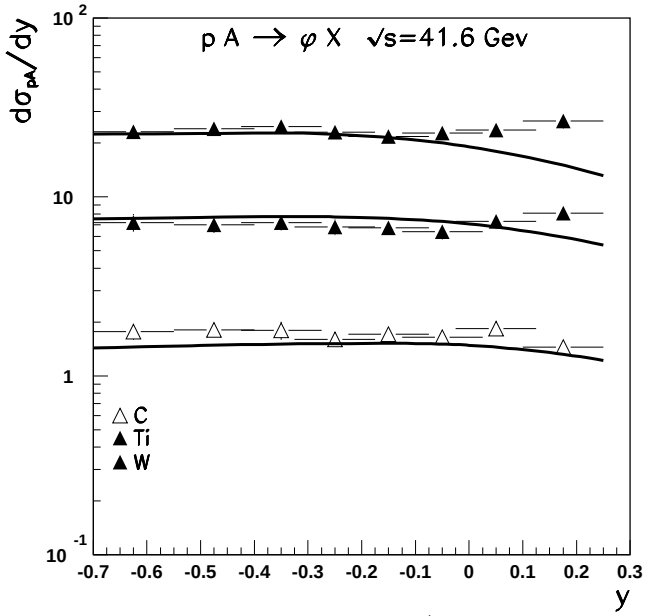

Figure 3: The experimental data on the y-spectra $d\sigma/dy$ of φ-mesons produced in proton-nucleus collisions on different (C, Ti, and W) nucleus at $\sqrt{s} = 41$ GeV [29], compared to the corresponding QGSM calculations.

inclusive density comes from the fact that the φ-meson has a significant mass, so the minimal values of $x_\pm$ in Eq. (3) noticeably decrease when the initial energy increases. This leads to the corresponding increase of the integration region in Eq. (4), and, consequently, to the increase of the inclusive density in the midrapidity region.

In Fig. 5 we compare the rapidity spectra dn/dy of the produced φ-mesons in PbPb collision at 158 Gev/c [31] with the results of the QGSM calculations. In principle, the agreement at y=0 is rather good, but the theoretical curve seems to fall down too fast with respect to the experimental data for $y > 0$.

5 The φ-meson production at LHC energies

In ref. [30] it was explained that starting from RHIC energies significant saturation effects for secondary production should be present in both pPb and PbPb collisions, what has been since generally accepted, both theoretically and experimentally [18, 36, 37].

At the same time, the spectra of secondaries produced in pp collisions were generally rather well described, without taking into account any saturation effects, even up to the range of LHC energies.

These saturation effects can be explained by the inelastic screening corrections connected to the multipomeron interactions [30], that at low energies are negligibly small due to the suppression of the longitudional part of the nuclear form factor. As this suppression of the longitudinal part of the nuclear form factor decreases whith the

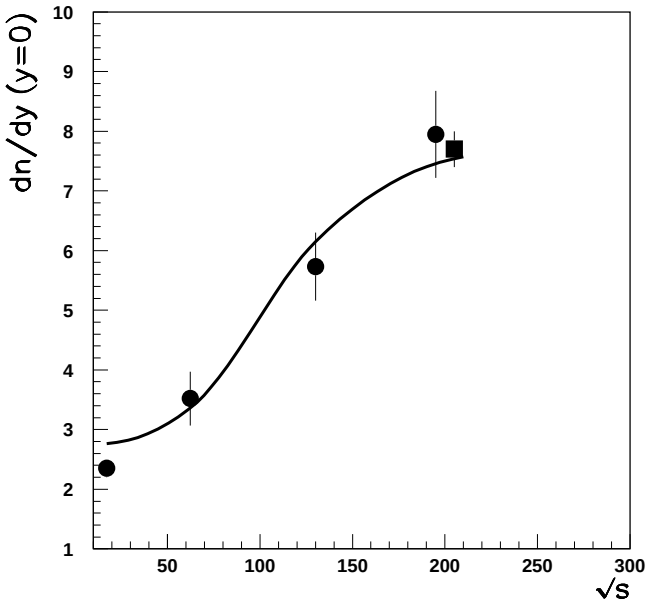

Figure 4: The experimental energy dependence of inclusive density of φ-mesons produced in the midrapidity region in both PbPb [31] and AuAu [32, 33, 35] collisions, together with the corresponding QGSM calculation.

growth of the initial energy, the inelastic screening corrections become more and more significant when the initial energy increases.

The calculations of inclusive densities and multiplicities, both in pp [38, 39] and in heavy ion collisions [39, 40] (with accounting for the inelastic nuclear screening), can be performed in the percolation approach, and they result in a good agreement with the experimental data for a wide energy region.

The percolation approach assumes that two or several Pomerons overlap in the transverse space and they fuse in a single Pomeron. Given a certain transverse radius, when the number of Pomerons in the interaction region increases, at least part of them may appear inside another Pomeron. As a result, the internal partons (quarks and gluons) can split, leading to the saturation of the final inclusive density. This effect will persist with the energy growth, until all the Pomerons will overlap [41, 42, 43].

In order to account for the percolation effects in the QGSM, it is technically more simple [18] to consider in the central region the maximal number of Pomerons, n_{max}, emitted by one nucleon. After they are cut, these Pomerons lead to the different final states. Then, the contributions of all the diagrams with $n \leq n_{max}$ are accounted for as at lower energies. The unitarity constraint would also allow the emission of a larger number of Pomerons $n > n_{max}$, but due to fusion in the final state (on the quark-gluon string stage) the cut of $n > n_{max}$ Pomerons would result in the same final state as the cut of n_{max} Pomerons.

With this prescription, the QGSM calculations become rather simple and very similar to those in the percolation approach. In this scenario, we obtain a reasonable agreement to the experimental data on the inclusive spectra of secondaries at RHIC

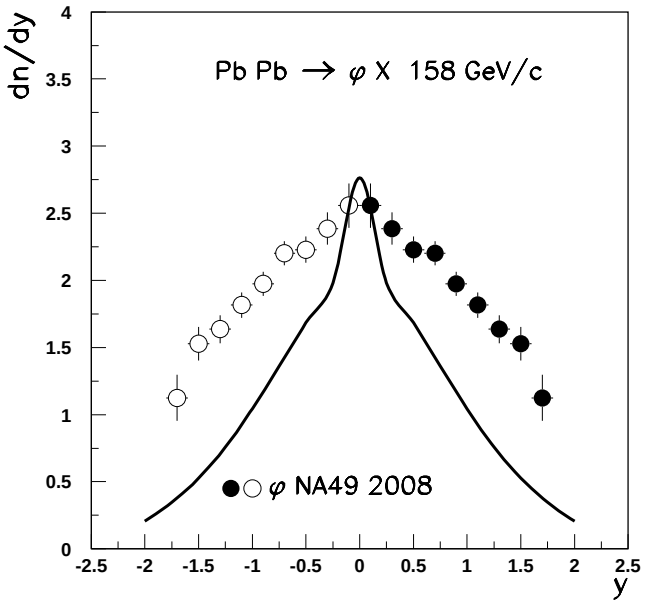

Figure 5: The experimental data on the rapidity spectra dn/dy of φ-mesons produced in PbPb collisions at 158GeV/c [31], compared to the QGSM calculations.

energy with a value $n_{max} = 13$ (see ref. [18]), and at LHC energies [17] with $n_{max} = 21$. The result that the number of strings for the secondary production increases with the initial energy, even when the percolation effects are included, was explained in ref. [44].

It was shown in the previous section that in the case of φ-meson production the inelastic shadowing effects are very weak at RHIC energy, being not visible inside the experimental error bars. Thus, we can assume that the φ-meson is produced from the cut of a Pomeron with relatively small transverse radius, so the overlapping and fusion of such a Pomeron occur with small probabilities, and they become significant only at very high energies. In such a picture, charm and beauty secondary particles would be produced from a Pomeron with very small transverse radius (large transverse momenta of partons), so saturation effects for charm and beauty secondaries should be many times smaller then for the φ-meson.

The experimental data for the inclusive densities of φ-mesons produced in central PbPb collisions were measured by the ALICE Collaboration [45] at the energy $\sqrt{s} =$ 2.76 Tev, and they are presented in Table 3. In QGSM, we obtain the value of dn/dy ($|y| \leq 0.5$) = 13.8, in agreement with the experimental data, for the value of n_{max}=37. The calculation with infinitely large n_{max}, i.e. without inelastic screening, gives the value dn/dy ($|y| \leq 0.5$) $\simeq 20.5$, so the inelastic screening effects for φ-meson production at $\sqrt{s} = 2.76$ Tev estimated by the QGSM turns out to be of $\simeq 1.5$.

The value of the parameter n_{max} was fixed as the result of the normalisation of QGSM calculations to the experimental data for dn/dy, $|y| \leq 0.5$. The rapidity dependence of dn/dy can be considered as the QGSM prediction. This rapidity dependence is shown in Fig. 6 by solid curve. For comparison, we also show our corresponding calculation without inelastic shadowing by a dashed curve.

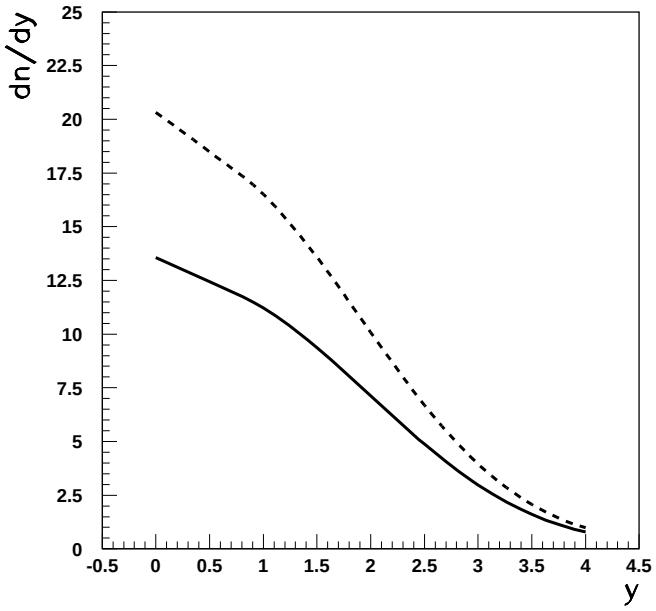

Figure 6: The QGSM prediction for the rapidity distribution of produced φ-mesons in central PbPb collisions at $\sqrt{s}$) = 2.76 Tev, with (solid curve) and without (dashed curve) inelastic screening.

Once the value of n_{max} is fixed, we can calculate the secondary φ-meson production in proton-nucleus and nucleus-nucleus collisions, without any additional parameter with respect to the corresponding calculations for pp collisions. Thus, also in Table 3 we present the QGSM predictions for φ-meson production in minimum bias PbPb collisions at $\sqrt{s} = 2.76$ Tev, and in pPb collisions at $\sqrt{s} = 5$ Tev.

Reactions	Centrality	Energy $\sqrt{s}$ TeV	Experimental data dn/dy, $\|y\| \leq 0.5$	QGSM
Pb + Pb	0−5%	2.76	$13.8 \pm 0.5 \pm 1.7 \pm 0.1$ [45]	13.57
Pb + Pb	minimum bias	2.76	−	3.98
p + Pb	minimum bias	5.0	−	0.16

Table 3: The experimental point on dn/dy, $|y| \leq 0.5$, on φ-mesons production in PbPb collisions at $\sqrt{s} = 2.76$ Tev, compared to the corresponding QGSM result, and together with the QGSM predictions for minimum bias production of φ-mesons on a Pb target.

6 Conclusion

Up to the RHIC energies, the QGSM provides a reasonable description of φ-meson production for the interactions of proton and nuclei with nuclear targets, without any additional parameters with respect to the case of pp collisions. The A-dependence of φ-meson production in proton-nucleus collisions presents the usual behaviour $d\sigma_{pA}/dy(y =$

0) $\propto A^1$, as it is shown in Fig. 2. The dependence of the φ-mesons production in midrapidity region on the initial energies is stronger than in the case of production of other hadrons. Also the inelastic screening effects are weaker for φ-mesons production, and they begin to be visible at higher energy $\sqrt{s}$ $\geq$1 Tev. Such a behaviour can be explained by the fact that the φ-mesons are produced in cut Pomerons with relatively small transverse radii. From the point of view of Reggeon Field Theory this means that the coupling of such a Pomerons to other Pomerons is weaker than the coupling of a Pomeron with standard transverse radii. This effect should be even stronger in the case of charm and beauty particle production, which are usually described in the frame of perturbative QCD.

Acknowledgements

We are grateful to M.G. Ryskin for useful discussions.

This work has been supported by Russian RSCF grant No. 14-22-00281, by the State Committee of Science of the Republic of Armenia, Grant-15T-1C223, by Ministerio de Ciencia e Innovación of Spain under project FPA2014-58293-C2-1-P, and the Spanish Consolider-Ingenio 2010 Programme CPAN (CSD2007-00042), and by Xunta de Galicia, Spain (2011/PC043).

References

[1] A.B. Kaidalov and K.A. Ter-Martorisyan, Sov. J. Nucl. Phys. **39**, 979 (1984) and Yad. Fiz. **39**, 1545 (1984); Sov. J. Nucl. Phys. **40**, 135 (1984) and Yad. Fiz. **40**, 211 (1984).

[2] A.B. Kaidalov, Phys. Atom. Nucl. **66**, 1994 (2003).

[3] A.B. Kaidalov, K.A. Ter-Martirosyan, and Yu.M. Shabelski, Sov. J. Nucl. Phys. **43**, 822 (1986) and Yad. Fiz. **43**, 1282 (1986).

[4] Yu.M. Shabelski, Z. Phys. **C38**, 569 (1988).

[5] Yu.M. Shabelski, Sov. J. Nucl. Phys. **50**, 149 (1989) and Yad. Fiz. **50**, 239 (1989).

[6] G.H. Arakelyan, C. Merino, C. Pajares, and Yu.M. Shabelski, Phys. Atom. Nucl. **76**, 316 (2013), Yad. Fiz. **76**, 1278 (2013), and arXiv:1207.6899hep-ph].

[7] A.B. Kaidalov and O.I. Piskounova, Sov. J. Nucl. Phys. **41**, 816 (1985) and Yad. Fiz. **41**, 1278 (1985).

[8] Yu.M. Shabelski, Sov. J. Nucl. Phys. **44**, 117 (1986) and Yad. Fiz. **44**, 186 (1986).

[9] G.H. Arakelyan, C. Merino, C. Pajares, and Yu.M. Shabelski, Eur. Phys. J. **C54**, 577 (2008) and hep-ph/0709.3174.

[10] G.H. Arakelyan, C. Merino, C. Pajares, and Yu.M. Shabelski, Eur. Phys. J. **A31**, 519 (2007) and hep-ph/0610264.

[11] G.H. Arakelyan, Sh.S. Eremian. Phys. Atom. Nucl. **58**, 1241 (1995), Yad. Fiz. **58**, 132 (1995).

[12] Sh.S. Eremian, Phys. Atom. Nucl. **59**, 135 (1996) and Yad. Fiz. **59**, 144 (1996)..

[13] G.H. Arakelyan, C. Pajares, and Yu.M. Shabelski. Z. Phys. **C73**, 697 (1997) and hep-ph/9602348.

[14] G.H. Arakelyan, C. Merino, and Yu.M. Shabelski, Phys. Rev. **D90**, 114019 (2014).

[15] G.H. Arakelyan, A. Capella, A.B. Kaidalov, and Yu.M. Shabelski, Eur. Phys. J. **C26**, 81 (2002) and hep-ph/0103337.

[16] G.H. Arakelyan, A.B. Kaidalov, C.Merino, and Yu.M.Shabelski, Phys. Atom. Nucl. **74**, 426 (2011) and arXiv:1004.4074[hep-ph].

[17] C. Merino, C. Pajares, and Yu.M. Shabelski, Eur. Phys. J. **C73**, 2266 (2013).

[18] C. Merino, C. Pajares, and Yu.M. Shabelski, Eur. Phys. J. **C59**, 691 (2009) and arXiv:0802.2195[hep-ph].

[19] G.H. Arakelyan, C. Merino, and Yu.M. Shabelski, Eur. Phys. J. **A52**, 9 (2016) and hep-ph/1509.05218.

[20] V.A. Abramovsky, V.N. Gribov, and O.V. Kancheli, Sov. J. Nucl. Phys. **18**, 308 (1974) and Yad. Fiz. **18**, 595 (1973).

[21] A.B. Kaidalov, Sov. J. Nucl. Phys. **45**, 902 (1987) and Yad. Fiz. **45**, 1452 (1987).

[22] Yu.M. Shabelski, Sov. J. Nucl. Phys. **26**, 573 (1977) and Yad. Fiz. **26**, 1084 (1977); Nucl. Phys. **B132**, 491 (1978).

[23] L. Bertocchi and D. Treleani, J. Phys. **G3**, 147 (1977).

[24] J. Weis, Acta Phys. Polonica **B7**, 85 (1977).

[25] T. Jaroszewicz *et al.*, Z. Phys. **C1**, 181 (1979).

[26] Yu.M. Shabelski, Z. Phys. **C57**, 409 (1993).

[27] J. Dias de Deus and Yu.M. Shabelski, Phys. Atom. Nucl. **71**, 190 (2008) Yad. Fiz. **71**, 191 (2008).

[28] G.D. Alkhazov *et al.*, Nucl. Phys. **A280**, 365 (1977).

[29] I. Abt *et al.*, HERA-B Collaboration, Eur. Phys. J. **C50**, 315 (2007).

[30] A. Capella, A. Kaidalov, and J. Tran Thanh Van, Heavy Ion Phys. **9**, 169 (1999).

[31] S.V. Afanasiev *et al.*, NA49 Collaboration, Phys. Lett. **B491**, 59 (2000); T. Anticic *et al.*, NA49 Collaboration, Eur. Phys. J. **C68**, 1 (2010).

[32] B.I. Abelev *et al.*, STAR Collaboration, Phys. Rev. **C79**, 064903 (2009).

[33] K. Adcox *at al.*, PHENIX Collaboration, Phys. Rev. **C69**, 024904 (2006).

[34] C. Adler *at al.*, STAR Collaboration, Phys. Rev. **C65**, 041901 (2002).

[35] J. Adams *et al.*, STAR Collaboration, Phys.Lett. **B612**, 181 (2005) and nucl-ex/0406003.

[36] B.B. Black *et al.*, PHOBOS Collaboration, Phys. Rev. Lett. **85**, 3100 (2000).

[37] K. Adcox *at al.*, PHENIX Collaboration, Phys. Rev. Lett. **86**, 500 (2001).

[38] I. Bautista, C. Pajares, and J. Dias de Deus, Nucl. Phys. **A882**, 44 (2012).

[39] I. Bautista, J. Dias de Deus, G. Milhano, and C. Pajares, Phys. Lett. **B715**, 230 (2012).

[40] I. Bautista, C. Pajares, G. Milhano, and J. Dias de Deus, Phys. Rev. **C86**, 034909 (2012).

[41] J. Dias de Deus, E. G. Ferreiro, C. Pajares, and R. Ugoccioni, Eur. Phys. J. **C40**, 229 (2005).

[42] C. Pajares, Eur. Phys. J. **C43**, 9 (2005).

[43] M.A. Braun, E.G. Ferreiro, F. del Moral, and C. Pajares, Eur. Phys. J. **C25**, 249 (2002).

[44] J. Dias de Deus and C. Pajares, Phys. Lett. **B695**, 211 (2012) and arXiv:1011.1099[hep-ph].

[45] B. Abelev *et al.*, ALICE Collaboration, Phys. Rev. **C91**, 0246609 (2015) and arXiv:1404.0495[nucl-ex].